Nano-electrochemistry & Nano-photochemistry
https://www.sciltp.com/journals/nenp

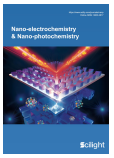

Article

A Broken Tip Allows a Better Trip: Translocation of Gold Nanoparticles Clusters through a Nanopipette

Qianyi Wu [1], Jian Lv [2,*] and Ruocan Qian [1,3,4,5,*]

[1] School of Chemistry & Molecular Engineering, East China University of Science and Technology, 130 Meilong Road, Shanghai 200237, China
[2] Faculty of Chemical Engineering and Energy Technology, Shanghai Institute of Technology, 100 Haiquan Road, Shanghai 201418, China
[3] Key Laboratory for Advanced Materials, East China University of Science and Technology, Shanghai 200237, China
[4] Feringa Nobel Prize Scientist Joint Research Center, Joint International Laboratory for Precision Chemistry, East China University of Science and Technology, Shanghai 200237, China
[5] Frontiers Science Center for Materiobiology & Dynamic Chemistry, School of Chemistry and Molecular Engineering, East China University of Science and Technology, Shanghai 200237, China
* Correspondence: lvjian@sit.edu.cn (J.L.); ruocanqian@ecust.edu.cn (R.Q.)

How To Cite: Wu, Q.; Lv, J.; Qian, R. A Broken Tip Allows a Better Trip: Translocation of Gold Nanoparticles Clusters through a Nanopipette. *Nano-electrochemistry & Nano-photochemistry* **2026**, *2*(2), 14. https://doi.org/10.53941/nenp.2026.100014

Received: 7 April 2026
Revised: 26 May 2026
Accepted: 16 June 2026
Published: 25 June 2026

Abstract: Nanopipette analysis is a sensitive sensing technology depending on the application of a potential to generate an ionic current at the orifice. Analytes such as DNA, proteins, and vesicles can be driven by the electric field inside the nanopipette, leading to detectable current blockage. However, it remains challenging to translocate negatively charged gold nanoparticles (AuNPs) through a conventional sharp nanopipette filled with symmetric physiological buffer. In this work, we introduce a strategy to drive the AuNPs out of the nanopipette tip conveniently without inner-wall functionalization. We intentionally break the nanopipette tip to change the geometry of orifice. Compared with intact nanopipettes, translocation events of AuNPs are significantly increased and detectable upon using nanopipettes with a broken-tip. This allows us to gain valuable insights into the driving force and translocation behaviour of AuNPs in nanopipettes with short necks and irregular edge at the tip. Our findings demonstrate a simple and effective strategy for AuNPs detection by nanopipettes and highlight the important role of tip geometry in pressure-assisted nanoparticle transport.

Keywords: nanopipette; tip geometry modification; pressure-assisted transport; ionic current sensing

1. Introduction

Single-molecule and nanoparticle sensing technologies are powerful tools for elucidating the microscopic mechanisms underlying biophysical and chemical processes [1–4]. Among various sensing platforms, nanopipette analysis has attracted considerable attention owing to its outstanding spatial confinement and high sensitivity [5–8]. This technique operates by applying a potential across the two ends of a nanopipette filled with electrolyte, thereby generating an ionic current at the nanometre-scale orifice [2,9]. When analytes such as DNA [10] and proteins are driven by the electric field through the nanopipette, they produce characteristic current blockade. Based on the amplitude and duration of these signals, qualitative analysis of the analytes can be achieved [11–14]. This method provides a novel approach for rapid, in-situ analysis in complex environments [5].

Gold nanoparticles (AuNPs), as functional nanomaterials integrating unique optical and electrical properties with biocompatibility, which are widely used in biological imaging [15–18], drug delivery [19,20] and disease diagnosis. In nanopipette sensing systems, AuNPs can serve not only as targeting probes for indirect detection of biomolecules, but also act as an ideal model for studying transport behaviour in nanoconfined spaces [21–23]. Although nanopipette-based detection of gold nanoparticles has been demonstrated in previous studies [24],

efficient transport of negatively charged gold nanoparticles through nanopipettes under symmetric physiological-buffer conditions and without inner-wall functionalization remains challenging [25]. To address this issue, conventional approaches usually rely on modifying the inner surface charge of nanopipettes to tune electroosmotic flow [26,27] or optimizing solution conditions [28]. However, these methods introduce additional chemical reaction steps, complex characterization, and potential batch-to-batch variability. They not only increase experimental complexity and cost, but also introduce interfering factors, thus obscuring the fundamental physical interactions between particles and pore channel. Therefore, it is highly desirable to develop a modification-free, operationally simple strategy for driving and detecting AuNPs.

In this work, we present a straightforward strategy based on physical alteration of tip geometry. We hypothesized that changing the tip structure could modify the transport pathway near the orifice a thereby improve the passage of negatively charged AuNPs. As illustrated in Scheme 1, we intentionally broken tip nanopipette as sensing probes, incorporating a two-electrode system (Ag/AgCl working as reference electrodes) and an external pressure-assisted setup to conduct the experiments. Experimental results demonstrate that, compared to intact sharp nanopipettes, broken-tip with shortened necks and irregular edges significantly increase the frequency of MPS-AuNPs cluster-induced blockade events. Overall, our strategy provides a simple and effective approach for AuNPs detection and offers an experimental model for understanding the influence of tip geometry on nanoparticle transport in nanopipettes.

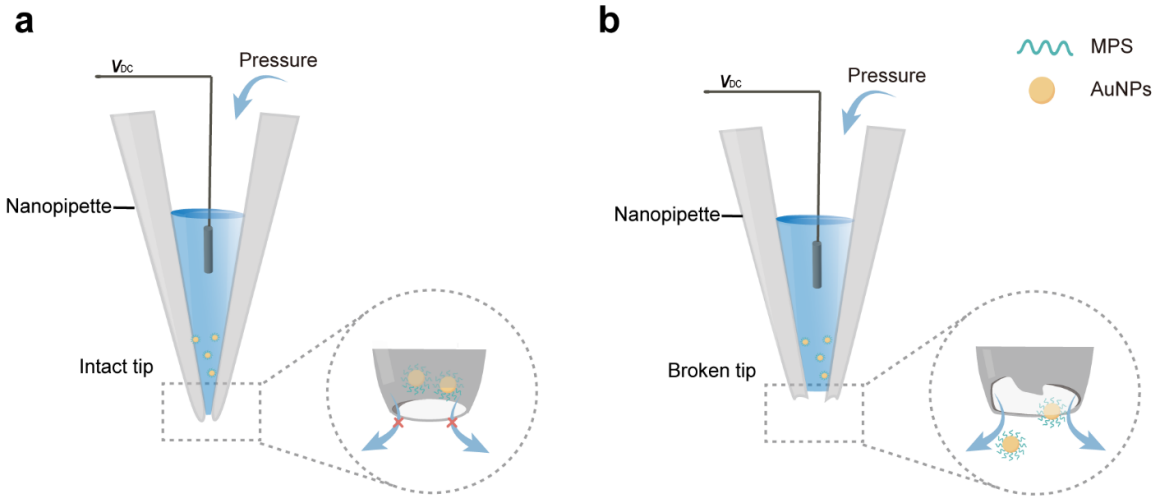

Scheme 1. Schematic illustration of the AuNPs detection strategy based on nanopipettes with different tip geometries: (**a**) intact tip and (**b**) broken tip.

2. Materials and Methods

2.1. Materials

Chloroauric acid ($HAuCl_4 \cdot 4H_2O$) was purchased from Shanghai Chemical Reagent Company (Shanghai, China). Trisodium citrate was obtained from Sinopharm Chemical Reagent Co., Ltd. (Shanghai, China). 3-mercapto-1-propanesulfonate (MPS) was purchased from Sigma. 1 × PBS buffer (pH 7.4) contained 136.7 mM NaCl, 2.7 mM KCl, 8.72 mM Na_2HPO_4, and 1.41 mM KH_2PO_4. Silver wires (0.25 mm) employed as electrodes in the experiments were obtained from Alfa Aesar. Quartz capillaries (OD: 1.0 mm, ID: 0.5 mm, 7.5 cm in length) were purchased from Sutter Instrument. All electrolyte solutions were prepared using ultrapure water with a resistivity of 18.2 MΩ, obtained from a Millipore water purification system (EMD Millipore, TONDINO, Shanghai, China).

2.2. Instruments

Dynamic light scattering (DLS) and Zeta potential analysis were performed on a Zetasizer (Nano ZS/ZS90, Malvern, UK). The UV-vis absorption spectra were obtained with a UV-vis spectrophotometer (Model 759S, Lengguang Tech, Shanghai, China). All reagents were weighed using an analytical balance (ME 104, Mettler Toledo, Greifensee, Switzerland). All reagents were centrifuged with a centrifuge (5430, Eppendorf, Hamburg, Germany). Nanopipettes were prepared using a P-2000 laser puller (Sutter Instrument, Novato, CA, USA). The SEM images of the nanopipettes and AuNPs were obtained by a field emission scanning electron microscope (Ultra 55, Carl Zeiss Ltd., Oberkochen, Germany). The nanopipette was secured under the microscope using a

holder (Axon Instruments, Union City, CA, USA) connected to an Axopatch 200B low-noise amplifier and an Axon Digidata 1550B low-noise data acquisition system (Molecular Devices, Sunnyvale, CA, USA) for electrochemical measurements.

2.3. Preparation of Gold Nanoparticles Probes

AuNPs with a diameter of approximately 60 nm were prepared according to a previously reported method [29]. Subsequently, 5 mL of the AuNPs solution was rapidly added to 5 mL MPS (200 μM). The mixture was reacted at room temperature for 30 min, followed by centrifugation at 5000 rpm for 5 min. The supernatant was discarded, and the precipitate was finally resuspended in 5 mL of deionized water.

2.4. Preparation of Glass Nanopipettes

Nanopipettes were fabricated using a laser puller with the following two-step program:

Line 1: Heat 650, Fil 3, Vel 30, Del 128, Pul 70;
Line 2: Heat 680, Fil 4, Vel 32, Del 132, Pul 130.

The cone-shaped nanopipettes were obtained and kept fresh before electrochemical sensing for the following experiments. For the preparation of broken-tip nanopipettes, the pulled nanopipettes were fixed on a sample stage at an appropriate angle. The nanopipette tip was manually broken by gently sweeping with a silver wire, and the tip morphology was monitored in real time using bright-field imaging.

2.5. Electrode Preparation

Two Ag/AgCl wires were introduced as electrodes to form a closed circuit for electrochemical signal acquisition. Silver wires were immersed in sodium hypochlorite solution for 30 min, resulting in the formation of a uniform and dense dark grey silver chloride (AgCl) coating on their surfaces, thus fabricating Ag/AgCl electrodes. The MPS-modified AuNPs were dispersed in PBS solution. A total of 10 μL of this dispersion was loaded into the nanopipette using a micropipette filler, followed by centrifugation at 3000 rpm for 2 min to remove air bubbles at the tip. The other Ag/AgCl electrode was immersed in 1 mM PBS buffer solution.

2.6. Measurement of Gold Nanoparticles Translocation Events

The nanopipette was stably mounted on a holder and connected to the headstage of an Axopatch 200B system. Acquisition and recording of electrochemical signals were performed using an Axopatch 200B amplifier coupled with a Digidata 1550B data acquisition system at a sampling rate of 100 kHz via pClamp 10.7 software (Axon Instrument, San Jose, CA, USA) installed on a computer. The experimental procedure was as follows: First, a petri dish containing 1 mM PBS (pH 7.4) was steadily placed at the centre of the microscope stage. The nanopipette was manipulated to move along the X, Y, and Z axes until it came into view under the microscope. The micromanipulator was switched to low-torque mode, and the Z-axis was carefully adjusted to fully submerge the nanopipette tip in the PBS buffer. After forming a stable electrochemical circuit, pressure was applied to the interior of the nanopipette using an external syringe. Meanwhile, pClamp 10.7 software was used to continuously record I-t (current-time) curves, and the interfacial dynamic changes at the nanopipette tip were synchronously monitored and recorded in real time via the microscope. Data fitting, statistical analysis, and image plotting were performed using MATLAB R2019a software (MathWorks, Natick, MA, USA).

3. Results and Discussion

3.1. Regulation and Characterization of the Tip Structure of Nanopipettes

The nanopipettes described in this study were fabricated by laser-pulling quartz capillaries. Optical and SEM images of the nanopipettes before and after tip breakage were shown in Figure 1a,b. Top view observations indicated that the tip diameter of an intact nanopipette is approximately 100 nm. After tip breakage, the tip size increased to the micrometre scale. The ionic fluxes of these two types of nanopipettes with different tip shapes were tested through current-voltage (I-V) curves, with the applied voltage scanned from −1000 mV to 1000 mV (Figure 1c,d) [30]. Compared with the intact-tip nanopipettes, the broken-tip nanopipettes demonstrated a weakened negative rectification effect, and the rectification ratio ($R = |I_{-1000\ mV}/I_{+1000\ mV}|$) decreased to 1.07 (Table S1). Based on the I-V curves measured at different times, no significant changes were observed after 30 min, indicating that the two types of nanopipettes showed good stability in the buffer solution (Figures S1 and S2; Table S2).

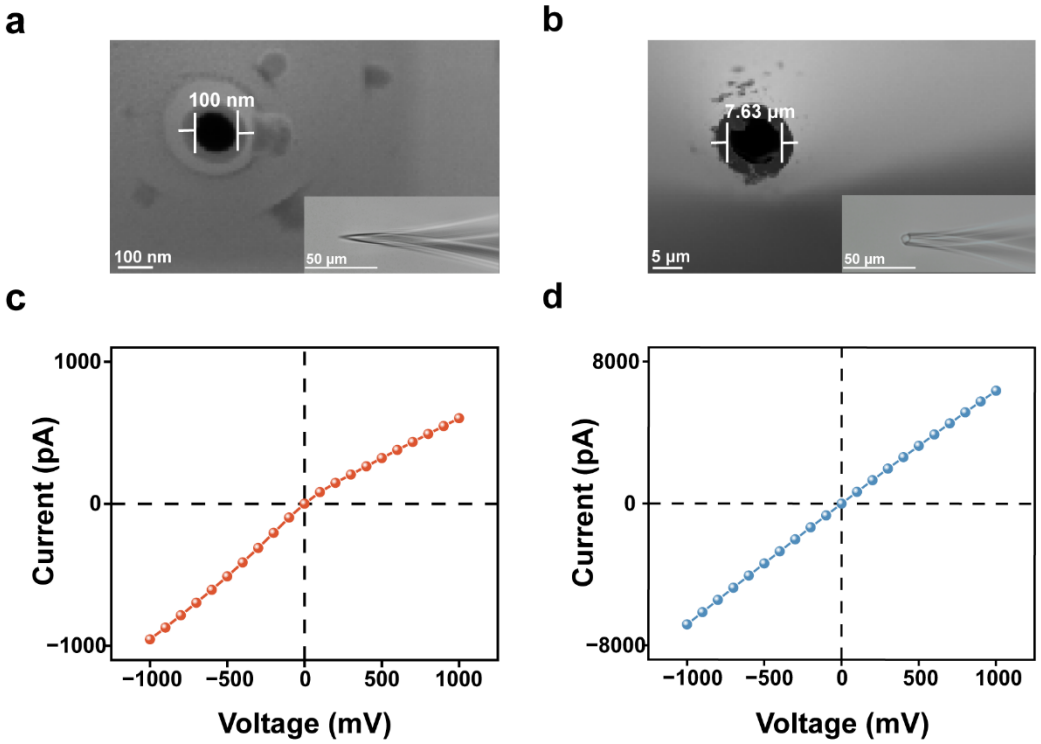

Figure 1. Characterization of the tip of the nanopipette before and after broken. Optical and scanning electron microscope images of (**a**) nanopipettes with intact tips and (**b**) nanopipettes with broken tips. I-V curves of nanopipettes (**c**) before and (**d**) after tip breakage (−1000 to 1000 mV).

3.2. Characterization of Gold Nanoparticles Probes

As the subsequent nanopipette experiments were conducted in PBS, AuNPs were also dispersed in PBS for characterization. Since bare AuNPs tended to aggregate in PBS because of reduced electrostatic repulsion, the particles were modified with MPS, and their properties before and after modification were compared. SEM (Ultra 55, Carl Zeiss Ltd., Oberkochen, Germany) images showed that both bare AuNPs and MPS-AuNPs were spherical, with diameters of approximately 60 nm, and no obvious change in morphology was observed after modification, indicating that MPS modification did not alter the basic morphology of the AuNPs (Figure 2a,b). To confirm the successful surface modification of AuNPs with MPS, X-ray photoelectron spectroscopy (XPS) was performed using an XPS spectrometer (K-Alpha+, Thermo Fisher Scientific, Waltham, MA, USA) to confirm the successful surface modification of AuNPs with MPS. MPS-AuNPs exhibited clear S 2p signals, confirming the introduction of sulfur-containing MPS onto the AuNP surface. The S 2p spectrum could be fitted with two spin-orbit doublets. The peaks at approximately 162 and 163 eV were attributed to Au-S bonds, indicating that MPS was anchored onto the AuNP surface through thiolate-gold interactions. The peaks at approximately 166 and 167 eV corresponded to the sulfonate group of MPS [31]. In addition, no obvious S 2p signal around 164 eV was observed, suggesting the absence of free or physically adsorbed thiol species (Figure S3). The results of DLS distribution showed that MPS-AuNPs exhibited a narrower size distribution than bare AuNPs (Figure 2c,d), suggesting a better dispersion after modification. The zeta potential showed that both bare AuNPs and MPS-AuNPs were negatively charged (Figure 2e), meaning the modification did not affect their negative surface charge. UV-vis spectra further showed that bare AuNPs displayed a broader absorption band with a tail at longer wavelengths in PBS, whereas MPS-AuNPs retained a clearer plasmon peak at around 540 nm (Figure 2f), consistent with reduced aggregation after modification. To further evaluate the colloidal stability of AuNPs in PBS, time-dependent UV-vis absorption spectra of bare AuNPs and MPS-AuNPs were measured after incubation in PBS for 0, 1, 3, and 6 h. After PBS addition, bare AuNPs solution gradually became aggregated (Figure S4a) and showed a broader plasmon absorption peak as the time increased, suggesting PBS-induced aggregation (Figure S4b). In contrast, MPS-AuNPs maintained a characteristic plasmon absorption peak at around 540 nm during incubation in PBS for 0, 1, 3, and 6 h, without obvious peak broadening (Figure S4c). These results indicated that MPS modification improved the stability of AuNPs in PBS, providing a suitable basis for the following nanopipette measurements.

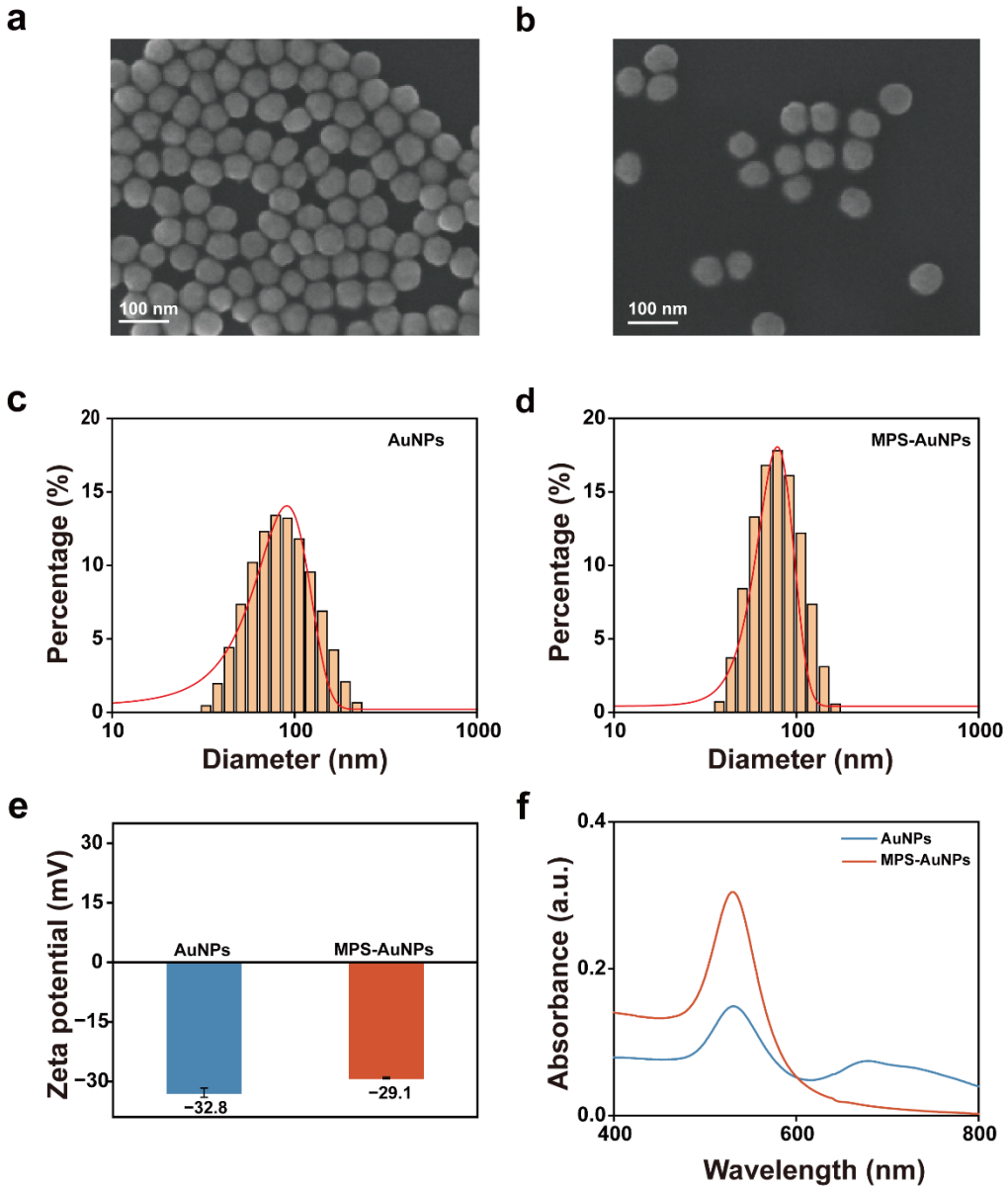

Figure 2. Characterization of bare AuNPs and MPS-modified AuNPs (MPS-AuNPs). SEM images of (**a**) bare AuNPs and (**b**) MPS-AuNPs. DLS size distributions of (**c**) bare AuNPs and (**d**) MPS-AuNPs. (**e**) Zeta potentials of bare AuNPs and MPS-AuNPs. (**f**) UV-vis absorption spectra of bare AuNPs and MPS-AuNPs in PBS.

3.3. Transport Behaviour and Current Signal Analysis of MPS-Modified AuNP Clusters

After the electrochemical platform had been established (Figure S5), we examined the transport behaviour of MPS-modified AuNPs under different tip geometries and driving conditions. As shown in Figure S6, no obvious blockade events were observed for intact-tip nanopipettes under an applied voltage. A similar result was obtained when broken-tip nanopipettes were tested under voltage alone (Figure S7). Pressure was then introduced as an auxiliary driving force. However, even under the combined application of voltage and pressure, intact-tip nanopipettes still failed to produce detectable translocation events (Figure S8). In contrast, transient blockade signals were observed only when voltage and pressure were simultaneously applied to broken-tip nanopipette. Since the tip opening became much larger after breakage, the recorded signals were not considered to arise from single nanoparticles, but more likely from the passage of MPS-modified AuNP clusters through the nanopipette tip. To further examine whether MPS-AuNP clusters were formed during the experiment, dark-field imaging was performed during pressure application. Enhanced scattering signals were observed near the broken-tip region, indicating pressure-induced the aggregation of MPS-AuNPs at the tip (Figure S9). These locally aggregated particles may pass through the broken-tip orifice in a cluster-like manner, resulting in the observed blockade signals.

Figure 3a showed a typical current-time (I-t) trace recorded during a single pressure cycle using a broken-tip nanopipette. The current trace could be divided into four parts (i–iv). At the beginning of the experiment, the

nanopipette tip was immersed in PBS buffer, and a stable baseline current was recorded before pressure applied (Figure 3a, part i). After pressure was applied, the gas flow from the syringe may disturb the nanopipette holder and cause a gradual upward shift of the baseline current (Figure 3a, part ii). As the pressure was further transmitted to the broken-tip, a series of blockade signals were observed on the I-t trace (Figure 3a, part iii). These signals were assigned to current blockade events associated with the passage of MPS-AuNP clusters through the broken-tip orifice, and representative events were shown in Figure 3c. After the pressure was released, the current gradually returned to the baseline level (Figure 3a, part iv).

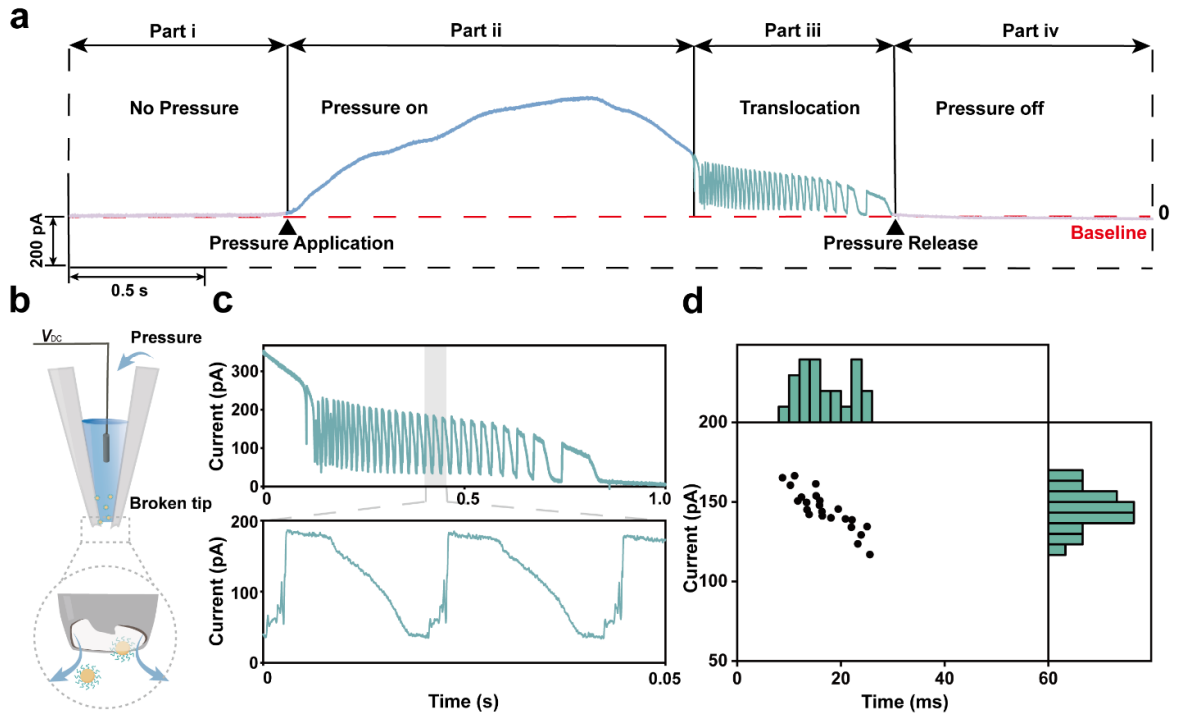

Figure 3. (**a**) Typical current-time (I-t) curve recorded during the application of pressure to a broken-tip nanopipette. Part i: baseline current. Part ii: pressure-induced baseline increase. Part iii: transient blockade events from MPS-AuNP clusters. Part iv: current recovery. (**b**) Schematic diagram of AuNPs translocation. (**c**) Blockade signals corresponding to the third segment in (**a**). (**d**) Scatter plot of blockade signal duration (x-axis) versus current (y-axis).

To confirm the origin of these signals, a blank control experiment was carried out under the same conditions using PBS without MPS-modified AuNPs in the nanopipette. No similar spikes were observed in the blank system (Figure S10), indicating that the applied pressure itself did not produce the recorded signals. Therefore, the events observed in part iii were assigned to the passage of MPS-modified AuNP clusters rather than to interference from pressure. Based on this result, the signals in part iii were chosen for the following statistical analysis. The corresponding scatter plot of blockade duration versus current change is shown in Figure 3d. These results indicate that detectable signals could only be obtained when pressure was applied to broken-tip nanopipette, indicating that tip geometry played an important role in the transport of MPS-modified AuNP clusters through the nanopipette.

4. Conclusions

In summary, we have developed broken-tip nanopipette for the pressure-assisted detection of MPS-modified AuNP clusters. Benefiting from the enlarged tip opening, the broken-tip nanopipette enabled measurable blockade signals, whereas intact-tip nanopipettes did not produce comparable responses under the same conditions. By combining pressure assistance, the passage of MPS-modified AuNP clusters could be monitored directly, and blank experiments further excluded interference from pressure itself. These results show that tip geometry plays an important role in particle-cluster transport through nanopipettes. This work provides a simple platform for studying nanoparticle transport in confined channels.

Supplementary Materials

The additional data and information can be downloaded at: https://media.sciltp.com/articles/others/2606251356425355/NENP-26040055-SI.pdf.

Author Contributions

Q.W.: literature review, manuscript preparation, and writing—original draft; J.L. and R.Q.: writing—review editing and supervision. All authors have read and agreed to the published version of the manuscript.

Funding

This work was supported by the National Natural Science Foundation of China (22504087), the Science and Technology Commission of Shanghai Municipality (24DX1400200, 25ZR1401082), the Program of Introducing Talents of Discipline to Universities (B16017), the Fundamental Research Funds for the Central Universities (222201717003) and Fundamental and Interdisciplinary Disciplines Breakthrough Plan of the Ministry of Education of China (JYB2025XDXM404). We thank the Research Centre of Analysis and Test of East China University of Science and Technology for their help on characterizations.

Data Availability Statement

All data are available in the article. Additional requests can be directed to the corresponding author.

Conflicts of Interest

The authors declare no conflict of interest.

Use of AI and AI-Assisted Technologies

No AI tools were utilized for this paper.

References

1. Actis, P.; Mak, A.C.; Pourmand, N. Functionalized Nanopipettes: Toward Label-Free, Single Cell Biosensors. *Bioanal. Rev.* **2010**, *1*, 177–185.
2. Albrecht, T. Single-Molecule Analysis with Solid-State Nanopores. *Annu. Rev. Anal. Chem.* **2019**, *12*, 371–387.
3. Stanley, J.; Pourmand, N. Nanopipettes—The Past and the Present. *APL Mater.* **2020**, *8*, 100902.
4. Yu, R.-J.; Ying, Y.-L.; Gao, R.; et al. Confined Nanopipette Sensing: From Single Molecules, Single Nanoparticles, to Single Cells. *Angew. Chem. Int. Ed.* **2019**, *58*, 3706–3714.
5. Denuga, S.; Dutta, P.; Duleba, D.; et al. Tuning Ion Current Rectifying Nanopipettes for Sensitive Detection of Methicillin-Resistant Staphylococcus aureus. *Anal. Chem.* **2025**, *97*, 2003–2010.
6. Kuanaeva, R.M.; Vaneev, A.N.; Gorelkin, P.V.; et al. Nanopipettes as a Potential Diagnostic Tool for Selective Nanopore Detection of Biomolecules. *Biosensors* **2024**, *14*, 627.
7. Song, J.; Xia, C.-W.; Zhang, X.; et al. A Modular DNA-Assembled Nanopipette (mDNP) Platform for Spatially Confined Single-Cell Nuclear Detection of Methyltransf erase Activity. *Anal. Chem.* **2025**, *97*, 21150–21157.
8. Zhang, X.; Wu, Z.-Q.; Zheng, Y.-W.; et al. Bridging Ionic Current Rectification and Resistive-Pulse Sensing for Reliable Wide-Linearity Detection. *Anal. Chem.* **2024**, *96*, 6444–6449.
9. Tian, S.-Y.; Gao, R.-X.; Du, Z.-Q.; et al. Dual-Interface Nanopipette Sensor for Electrochemical Interferent Shielding. *Angew. Chem. Int. Ed.* **2025**, *64*, e202504520.
10. Fraccari, R.L.; Ciccarella, P.; Bahrami, A.; et al. High-Speed Detection of DNA Translocation in Nanopipettes. *Nanoscale* **2016**, *8*, 7604–7611.
11. Demirtas, M. Enhancing the Sensitivity of Nanopipette Biosensors for Protein Analysis. *Brain Behav.* **2024**, *14*, e3405.
12. Lv, J.; Wang, X.-Y.; Chang, S.; et al. Amperometric Identification of Single Exosomes and Their Dopamine Contents Secreted by Living Cells. *Anal. Chem.* **2023**, *95*, 11273–11279.
13. Yu, R.-J.; Ying, Y.-L.; Hu, Y.-X.; et al. Label-Free Monitoring of Single Molecule Immunoreaction with a Nanopipette. *Anal. Chem.* **2017**, *89*, 8203–8206.
14. Zhang, X.; Luo, D.; Zheng, Y.-W.; et al. Translocation of Specific DNA Nanocarrier through an Ultrasmall Nanopipette: Toward Single-Protein-Molecule Detection with Superior Signal-to-Noise Ratio. *ACS Nano* **2022**, *16*, 15108–15114.
15. Jain, P.K.; Huang, X.; El-Sayed, I.H.; et al. Noble Metals on the Nanoscale: Optical and Photothermal Properties and Some Applications in Imaging, Sensing, Biology, and Medicine. *Acc. Chem. Res.* **2008**, *41*, 1578–1586.

16. Karnwal, A.; Kumar Sachan, R.S.; Devgon, I.; et al. Gold Nanoparticles in Nanobiotechnology: From Synthesis to Biosensing Applications. *ACS Omega* **2024**, *9*, 29966–29982.
17. Qian, X.; Peng, X.-H.; Ansari, D.O.; et al. In Vivo Tumor Targeting and Spectroscopic Detection with Surface-Enhanced Raman Nanoparticle Tags. *Nat. Biotechnol.* **2008**, *26*, 83–90.
18. Saha, K.; Agasti, S.S.; Kim, C.; et al. Gold Nanoparticles in Chemical and Biological Sensing. *Chem. Rev.* **2012**, *112*, 2739–2779.
19. Dykman, L.; Khlebtsov, B.; Khlebtsov, N. Drug Delivery Using Gold Nanoparticles. *Adv. Drug Deliv. Rev.* **2025**, *216*, 115481.
20. Ghosh, P.; Han, G.; De, M.; et al. Gold Nanoparticles in Delivery Applications. *Adv. Drug Deliv. Rev.* **2008**, *60*, 1307–1315.
21. Lan, W.-J.; Holden, D.A.; Zhang, B.; et al. Nanoparticle Transport in Conical-Shaped Nanopores. *Anal. Chem.* **2011**, *83*, 3840–3847.
22. Ramirez, A.B.; Lazenby, R.A. Fabricating Reproducible, Reversible, and High Signal Change Aptasensors with Gold-Modified Nanopipettes. *ACS Appl. Mater. Interfaces* **2025**, *17*, 24877–24886.
23. Zhou, Y.; Wang, D.; Li, C.; et al. Resistive-Pulse Sensing and Surface Charge Analysis of a Single Nanoparticle Collision at a Conical Glass Nanopore. *Anal. Chem.* **2019**, *91*, 7648–7653.
24. Zheng, X.; Liu, J.; Li, M.; et al. Dual-Nanopipettes for the Detection of Single Nanoparticles and Small Molecules. *Anal. Chem.* **2022**, *94*, 17431–17438.
25. Wei, R.; Gatterdam, V.; Wieneke, R.; et al. Stochastic Sensing of Proteins with Receptor-Modified Solid-State Nanopores. *Nat. Nanotechnol.* **2012**, *7*, 257–263.
26. Sa, N.; Baker, L.A. Rectification of Nanopores at Surfaces. *J. Am. Chem. Soc.* **2011**, *133*, 10398–10401.
27. White, H.S.; Bund, A. Ion Current Rectification at Nanopores in Glass Membranes. *Langmuir* **2008**, *24*, 2212–2218.
28. Ma, L.; Li, Z.; Yuan, Z.; et al. Modulation of Ionic Current Rectification in Ultrashort Conical Nanopores. *Anal. Chem.* **2020**, *92*, 16188–16196.
29. Zhang, P.; Li, Y.; Wang, D.; et al. High-Yield Production of Uniform Gold Nanoparticles with Sizes from 31 to 577 nm via One-Pot Seeded Growth and Size-Dependent SERS Property. *Part. Part. Syst. Charact.* **2016**, *33*, 924–932.
30. Yusko, E.C.; An, R.; Mayer, M. Electroosmotic Flow can Generate Ion Current Rectification in Nano- and Micropores. *ACS Nano* **2010**, *4*, 477–487.
31. Venditti, I.; Fontana, L.; Scaramuzzo, F.A.; et al. Nanocomposite Based on Functionalized Gold Nanoparticles and Sulfonated Poly (Ether Ether Ketone) Membranes: Synthesis and Characterization. *Materials* **2017**, *10*, 258.